Using Weak Light Sources to Power Sensor Nodes for Sustainable IoT

Mingzhe Li[1], Zhen Xiao[1], Cui Zhao[2], and Zhenjiang Li[1]
[1]Department of Computer Science, City University of Hong Kong, China
[2]Faculty of Electronic and Information Engineering, Xi'an Jiaotong University, China

***Abstract*—This paper introduces a novel Internet of Things (IoT) node design, WISE, which can operate autonomously using weak light sources, e.g., indoor lights or weak sunlight. As IoT systems are increasingly deployed, a fundamental question is drawing attention: How can we sustainably power the vast number of IoT nodes? Traditional batteries are insufficient due to their limited lifetime and high replacement costs in scalable IoT systems. Energy harvesting thus recently emerged as a promising solution, where nodes can harvest enough energy from outdoor sunlight. Regarding recent works, this paper focuses on an important but understudied segment of deployment scenarios that mainly contain weak light sources, e.g., indoors where lamps are the main light source. Our key innovation for powering nodes using weak light sources is a new node architecture featuring a timing supply control part, reducing quiescent current to nano-ampere (nA) levels, and optimizing energy use. We further propose a scheme to optimize the selection of hardware components in customizing WISE nodes, according to different design requirements, and an energy-aware scheduling method. We develop and test three WISE node configurations in real-world environments, achieving substantial improvements in communication rate and energy efficiency compared to the state-of-the-art node designs.**

I. Introduction

The Internet of Things (IoT) is reshaping the way people live and interact, characterized by the convergence of the physical and digital realms. Due to its importance in building smart cities, IoT nodes have grown rapidly over the past few decades, reaching 40+ billion in 2023 [39], three times that of 2018, and is expected to increase to one trillion by 2035 [33]. However, as the scale of IoT nodes with rich functions (sensing, computing, and communication) extends exponentially, a fundamental challenge for the ubiquitous deployment of IoT systems arises — *how to sustainably power these IoT nodes?*

Applications often require sufficient flexibility in node deployment [45], such as in outdoor, rural, or mobile scenarios, where cables (connected to the grid) are not feasible. Commonly adopted batteries are also no longer suitable due to their limited lifetime. For example, even with the latest low-power wireless modules (*e.g.*, LoRa [38] or Bluetooth [3]), they consume 0.01–0.1 mA in sleep mode and 15–40 mA in active mode. Assuming a very low duty cycle of 1% (asleep for 99% of the time), a standard 3000 mAh battery can only power the wireless module for 8–26 months. Sensing, computing, or higher duty cycles will further shorten the device's lifetime, requiring frequent battery replacement. When the number of nodes is large, the cost of battery replacement or recharging is very high, making IoT systems unable to work autonomously.

To overcome this issue, a promising solution is to power IoT devices by harvesting energy from the device's surroundings (*e.g.*, light) without using batteries. Energy-harvesting IoT nodes can recharge their energy storage (*e.g.*, supercapacitors) in an autonomous and self-service manner without human intervention. This family of designs has made rapid progress recently due to breakthroughs in two areas [36], [51]. First, solar panels now can be miniaturized and maintain good energy conversion efficiency, making them feasible to power IoT nodes. Second, research in intermittent computing provides effective techniques to schedule sensing and communication tasks and reduce system errors or failures (see Section VI). So far, energy-harvesting IoT nodes have been successfully deployed in various outdoor environments [31], and may also be deployed in outer space in the near future [27].

In this paper, we focus on a very important but under-studied segment in energy-harvesting IoT node deployment scenarios, which often contain only weak light sources. Typical examples are various indoor environments, where the main light source is lamps. As a core pillar of the IoT ecosystem, smart buildings are in great need of IoT coverage. To deploy IoT systems on a large-scale indoors, nodes are usually expected to be installed in a plug-and-play manner anywhere in the building where they need to sense. So that they can directly harvest energy from the ambient weak light sources to power themselves (without connecting to any power cords or regularly replacing batteries). In fact, similar deployment convenience is also required in many outdoor environments, such as in woods or forests without sufficient sunlight coverage. However, using weak light sources to power IoT nodes face two major challenges:

1) Device energy leak: Idle IoT nodes still consume considerable energy. For example, the quiescent current of the node is in the sub-mA level [10], [11], [28] (*i.e.*, the current when the node is idle). Although it is much smaller than the working current, when the power supply is weak, this quiescent current will consume a large proportion of the stored energy, causing the node to be in an energy-deficient state most of the time, thus affecting the node's operation.

2) Energy intermittency: In addition to the limited intensity of weak light sources, the complexity of real-world deployment brings another challenge, characterized by the highly dynamic nature of energy supply and consumption, which makes it more difficult to ensure that nodes can perform smoothly 7/24 under various lighting conditions [36].

While emerging energy-harvesting materials such as per-

ovskite solar cells [13] have been proposed for a higher energy conversion efficiency, they are mainly in the laboratory stage and have not yet been mass-produced. On the other hand, energy harvesting from radio frequency (RF) signals is also an emerging technology (*e.g.*, using RFID [23], [37], [52] or Wi-Fi [22]), but its energy intensity is too low for IoT devices with multiple modules and functions [19], and also requires additional RF equipment to support.

In this paper, we show that it is possible to use small commercial off-the-shelf (COTS) solar panels to power sensor nodes for autonomous operation in weak light sources (*e.g.*, indoor lights or weak sunlight). Our key innovation is a new IoT node design that includes a novel ultra-low power architecture for connecting and managing power and onboard components (*e.g.*, sensors, computing modules, wireless modules, *etc.*). The main reason why most IoT nodes have high quiescent power consumption is that the nodes reuse the timer in the microcontroller (MCU) to control the timing of the node, such as the sleep and wake-up of the node. However, since the MCU is a computing component, it consumes considerable energy even in low-power states, which is the main reason for the high quiescent current in existing IoT nodes.

Therefore, we design an ultra-low power component specifically for controlling the device timing. When the node is asleep, the MCU can also be completely turned off, making the quiescent current only in the nA level, so that almost all the energy harvested by the node can be used for operation. Based on this idea, we enable matching and compatibility of the separate timing control part for the energy harvesting, storage, and voltage regulation components. In addition, we design an optimization scheme that can select the best combination of key hardware components according to different deployment requirements, such as node cost, performance, or a balance between the two, during the node production stage. Finally, we design an energy-aware scheduling method to manage the harvested energy to ensure a smooth operation of the node under different lighting conditions.

We implement the design of using weak light sources to power IoT nodes in a system, called WISE. The node size is 36.1mm $\times$ 36.7mm, as shown in Fig. 1. It uses COTS solar panels and supercapacitors to harvest and store energy, and uses an external RTC chip in our proposed timing control part to achieve ultra-low quiescent current. Each node also includes a MCU for computing, a light sensor and an image sensor for sensing, and a LoRa transceiver for communication. We further reserve interfaces to install more sensors in the future. To evaluate its performance, we develop three instances of the WISE node by using hardware components of different configurations (*e.g.*, prioritizing node cost, performance, and a balance between the two). In addition, we also develop two state-of-the-art energy-harvesting node designs SMARTON [28] and ACES [10] as baselines. We deploy all nodes in two typical weak light environments, including an indoor office and outdoor woods, with average illumination ranging from 400 to 560 Lux. Extensive experiments show that WISE can improve the quality of service (*e.g.*, communication rate) by 69.7–185.2% and an energy efficiency increase of 64.3–192.0%. In summary, this paper makes the following contributions:

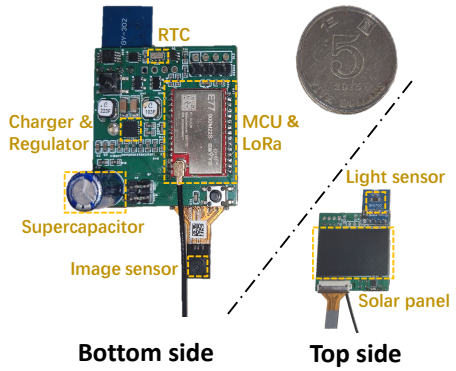

Fig. 1. Prototype of WISE with the main PCB size of about 36.1mm$\times$36.7mm.

- We propose a novel IoT node design with ultra-low power consumption that can power itself using weak light sources for autonomous sensing and communication.
- We design a full-stack solution that encompasses both hardware and software designs to accommodate the dynamics of energy supply and consumption.
- We develop prototypes of WISE nodes, deploy them in real-world environments and compare them with state-of-the-art designs to show significant performance gains.

II. Background and Problem Statement

A. Energy Harvesting from Weak Light Sources

Outdoor sunlight intensity is usually above 10,000 Lux, and IoT nodes can easily harvest energy from sunlight to power themselves and store enough energy for future use [51], *e.g.*, at night. However, in many outdoor scenarios with severe obstruction, such as monitoring in woods or forests, the peak light intensity may drop below 1,000 Lux [2], and the average intensity during the day is only a few hundred Lux, resulting in significantly reduced energy availability. This not only affects the energy harvesting required to power IoT operations, but also poses challenges to energy storage, which increases the possibility of node failures under extreme weather conditions.

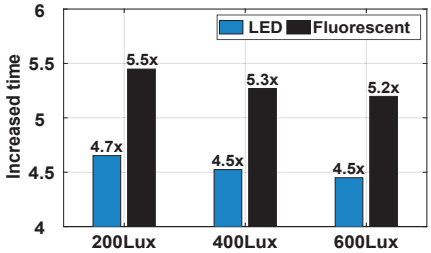

Fig. 2. At the same light intensity, the increased ratio of using LED and fluorescent lamps to harvest the same energy compared to that of using sunlight.

This problem may become more serious when nodes are deployed indoors (such as office buildings, smart homes, and underground coal mines) and expect to harvest energy from artificial light sources (such as various lamps). Although

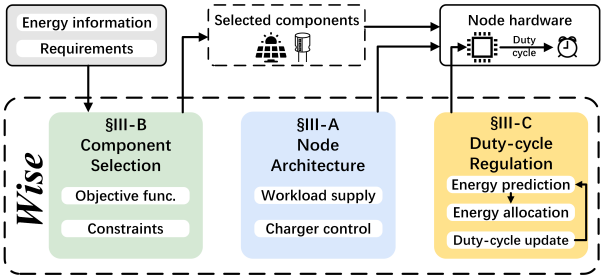

Fig. 3. Overview of the WISE design.

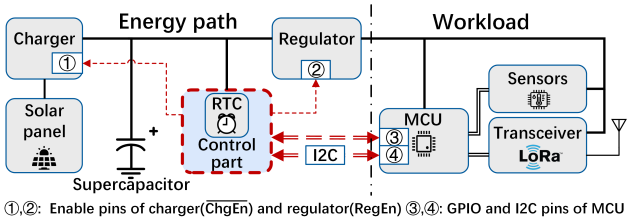

Fig. 4. WISE contains a separate timing control part (red dashed box) and four connection lines (red dashed lines) to reduce the quiescent current.

lamps can provide relatively stable illumination (compared to sunlight), their intensity is much weaker, usually between 100 and 600 Lux. More importantly, the efficiency of energy harvesting is much lower than that of sunlight. This is because the energy from sunlight greatly exceeds the invisible bands of the human eye, and solar panels can also harvest energy from these invisible bands. In contrast, the energy of artificial light is mainly concentrated in the visible light band [24], and the overall collectable energy is 80–86% lower than sunlight at similar lighting levels. As Fig. 2 shows, under similar lighting levels, it takes 4.5–4.7 and 5.2–5.5 times longer to harvest the same amount of energy (*e.g.*, 50 mJ) using LEDs and fluorescent lamps than using sunlight, respectively.

Finally, given that light sources are not always available, such as after turning off the lights, harvesting sufficient energy from weak light sources becomes more challenging in practice.

B. Energy Consumption of Sensor Nodes

At the energy-harvesting IoT node, the harvested energy is consumed primarily in the following ways.

1) Operations. Sensing and communication are the parts that consume the most energy during node operation. Traditional sensors (such as light sensors) consume $\sim$11μJ (at 3 V) per reading, while more complex sensors (such as image sensors) consume 3.3 mJ (at 3 V) per reading. Compared with sensing, communication requires more energy. Taking the widely used LoRa as an example, it takes $\sim$16 mJ (at 3 V) to transmit a 25-byte data packet under the common setting of a spreading factor of 8 and a transmission power of 10 dBm.

2) Quiescent current. Another major energy consumption in energy-harvesting nodes is quiescent current, which is a waste of energy when the node is idle and is typically greater than 5 μA using state-of-the-art designs [10], [28]. At existing quiescent current levels, the energy to support one time of sensing and communication can leak out in 21.7 minutes.

Therefore, it is challenging to ensure stable and autonomous operation of nodes under weak-light conditions, which we will address in the next section by proposing WISE.

III. WISE Design

Fig. 3 overviews the WISE design with three main modules:

- **Node architecture (Section III-A)**: a new node architecture design with a dedicated timing control part that achieves ultra-low quiescent current by using an external real-time clock (RTC) and corresponding control logic.
- **Component selection (Section III-B)**: an optimization scheme to select the best combination of several key energy-related components based on different design requirements during the node production stage.
- **Duty-cycle regulation (Section III-C)**: an energy-aware duty-cycle regulation method used to prudently consume harvested energy, thereby enabling sustainable IoT services under weak light sources.

Next, we elaborate the design of each module in WISE.

A. Node Architecture

Traditional energy-harvesting sensor nodes usually consist of two main parts: the *energy path* and the *workload*, as shown in the Fig. 4 (except for the parts marked by red). In the energy path, a solar panel (or other energy source) is usually used to collect energy and store it in a supercapacitor through a charger, while a voltage regulator ensures a stable and consistent voltage output (such as 3 V) for the workload. With proper energy supply, the MCU commands the transceiver to transmit sensor data through a wireless module (such as LoRa). Subsequently, both the sensor and the transceiver enter sleep mode until a wake-up interrupt is triggered to save energy. However, existing energy-harvesting sensor node designs still have non-negligible energy consumption, affecting the node performance under weak-light conditions.

Problem. In the sleep mode of an energy-harvesting node, there is still a mild but continuous energy consumption, namely the *quiescent current* (in the μA level in existing designs [10], [28]), to ensure that the node can respond to the wake-up trigger. This energy consumption is relatively weak, so it is easy to be ignored. However, since the quiescent current continues to occur, it can cause performance degradation when light is weak, such as being unable to store enough power for sensing and communication for a long time or even a power failure. Therefore, it is urgent to solve this problem to provide sustainable node operations.

Solution. Through our investigation, we find that the main reason for the high quiescent current is that the nodes reuse the timer in the MCU to control the timing of the nodes and their awake and sleep states. However, since the MCU is a computing component, it consumes considerable energy even in sleep mode. To overcome this problem, our main idea is to introduce a dedicated timing control part based on an external real-time clock (RTC), so that the quiescent current from the MCU can be cut off by delegating the timing function to the RTC component. Specifically, the control part receives

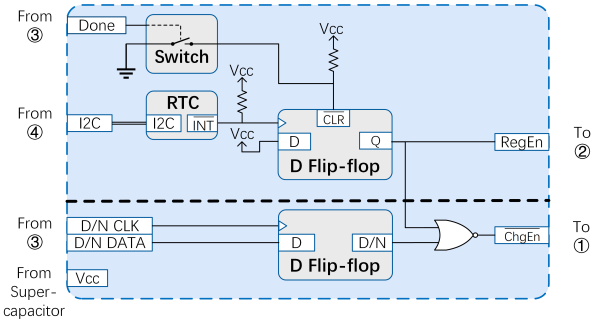

Fig. 5. Design of the control part in WISE, where ① – ④ correspond to the same numbers in Fig. 4.

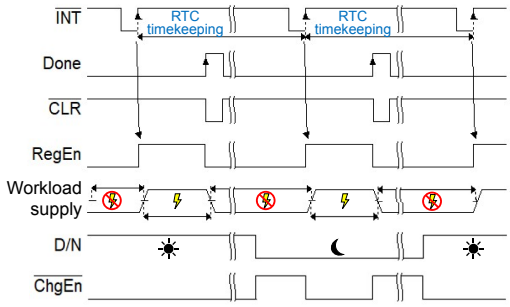

Fig. 6. Timing diagram of each component of the control part.

commands from the MCU through the GPIO (general-purpose input/output) and I2C bus, shown as ③,④ in Fig. 4. Based on these commands, the control part can generate customized timing signals separately to handle the power supply from the charger and regulator to the workload. When the system is turned into sleep mode, the quiescent current (originally from the MCU) is effectively eliminated, and the quiescent current of the RTC is only 45 nA.

The above is the overall idea of our node architecture design. Next, we elaborate on the details of the control part so that it can work organically with the workload and energy path.

1) Workload supply control: Harvested solar energy is converted into electrical energy and stored in the supercapacitor, but the voltage of the supercapacitor fluctuates greatly and cannot be directly used to power the workload. Thus, we first use an external RTC (*e.g.*, RV3028-C7) as the basic control part, which can support a wide supply voltage of 1.1V to 5.5V without the need for an additional voltage regulator. Subsequently, in order to provide a steady-state output for the workload, we must further reshape the control part design and add some suitable logic elements, because the commercial RTC can provide valid pulses for a few milliseconds only.

To this end, in the control part, the sub-part above the dashed line in Fig. 5 receives the "Done" signal as well as I2C bus command from the MCU (③,④ in Fig. 4), and outputs the workload supply command ("RegEn") to the regulator. Specifically, when the node is in low-power sleep mode, the RTC maintains the timing function. Once the system's sleep mode timer expires, the RTC generates a pulse to reset the active-sleep cycle. The rising edge of this pulse (the upward arrow in the $\overline{\text{INT}}$ row in Fig. 6) will be captured by the D flip-flop and instruct the regulator to start the workload and activate the sensor node to perform tasks by outputting a stable high-level signal (high level in the "RegEn" row in Fig. 6) to the regulator enable pin (② in Fig. 4). When the task is complete, the control part receives a "Done" pulse (from the MCU) that pulls down the asynchronous clear pin of the D flip-flop ("$\overline{\text{CLR}}$" in Fig. 5) via the normally open switch. It clears the regulator enable signal, which cuts off power to the workload and switches the sensor node back to sleep mode.

2) Charger's control: After avoiding the quiescent current that the MCU continues to accumulate, we observe some residual energy consumption caused by the charger, which needs to be further eliminated. For example, even if we use advanced power management chips (such as TI's BQ25570), its charger still generates a quiescent current of 450–600 nA. Although we usually ignore such a weak current under strong lighting conditions, this quiescent current consumption is still serious at night or when there is not enough energy income.

To address this issue, we design an enable/disable control logic for the charger. As shown below the dashed line in Fig. 5, another D flip-flop determines whether the charger should be turned on or off. Specifically, this D flip-flop storage has a value ("D/N" in Fig. 6) preset by the MCU through the clock and data lines ("D/N CLK" and "D/N DATA" in Fig. 5, from ③ in Fig. 4), which are determined by the ambient energy availability. To use the D/N value as the enable/disable signal for the charger ($\overline{\text{ChgEn}}$), we further include a NOR gate to meet the specific configuration requirements of the charger. As shown in Fig. 6, $\overline{\text{ChgEn}}$ linked to ① in Fig. 4 shows a low value (enabling the charger) during the day and the opposite at night (except for the active mode time). This design can effectively shut down idle chargers at night, further saving energy for sensing and communication tasks.

Summary of WISE's quiescent current. According to our measurement, the WISE design (including RTC, switch, logic gates, and two D flip-flops) only results in an ultra-low quiescent current of about 60 nA. Except for the RTC chip (no more than 45 nA @3V), all other components are CMOS components, and their quiescent current is less than 10 nA in total. Moreover, if the charger is turned on, this quiescent current consumption can be 450–600 nA, but it is 5–10 μA in the SOTA designs for the energy-harvesting nodes [10], [28].

B. Component Selection

The node architecture proposed above is a general design. Building on this, we further address a practical problem encountered in designing and producing WISE nodes. Once the sensors and wireless modules on the node are determined, we find that the node behaves very differently when different configurations of energy-related components are selected, such as solar panels and supercapacitors. Therefore, depending on the different requirements of IoT system deployment, such as whether to prioritize node cost, performance, or a balance between the two, we should choose the optimal configuration of these components to meet the deployment requirements. We design this optimization scheme in this subsection.

Objective. For each component i, denote p_i as the set of its possible parameters that can be used to design the WISE node. We aim to select decision variables p, where $\mathrm{p} = \{p_i\}$, to optimize the following objective function by considering the cost c_{p_i} and the energy income-to-consumption ratio r_p:

$$\arg\max_{\mathrm{p}}\left(\frac{w}{\sum_i c_{p_i}} + (1-w)\times r_\mathrm{p}\right), \tag{1}$$

where w is a factor within $[0,1]$ that is used to balance the weights of the cost and energy ratio. In Eqn. (1), the first term $\sum_i c_{p_i}$ is the total cost of the selected components, which is expected to be small usually. The second term r_p measures the potential richness of energy storage, which is expected to be large usually and is calculated as the ratio between energy income E_{in} and energy consumption E_{con} as follows:

1) Energy income E_{in}: we first estimate the (minimum) energy income level for the deployment site, which together with the energy consumption below provides a practical constraint and reference for the selection of solar panel and supercapacitor. For indoor environments, the light energy Q per unit area on the solar panel over a day can be obtained through field measurements or estimated based on the type of light source and the distance from the node to the light. For outdoor environments, Q can be obtained through field measurements or light records from local weather stations, where we can use the minimum value recorded to provide a conservative estimate. Then, E_{in} can be obtained as follows:

$$E_{in} = Q \times s_{p_{sp}} \times \eta_{p_{sp}} \times \eta_{p_{sc}}, \tag{2}$$

where $s_{p_{sp}}$ is the size of the chosen solar panel, $\eta_{p_{sp}}$ and $\eta_{p_{sc}}$ are the energy conversion efficiencies of the solar panel and supercapacitor, respectively. They can be found in the hardware specifications of these components.

2) Energy consumption E_{cn}: the energy consumption of a node includes the continuous quiescent energy consumption (E^q_{cn}) caused by the quiescent current and the operating energy consumption (E^o_{cn}) of periodic sensing and communication. We can express E_{cn} ($= E^q_{cn} + E^o_{cn}$) further as:

$$E_{cn} \quad = \quad (V \times I_q) \times T + (\sum\nolimits_j E^{o,s}_{cn}(j) \times l) \times T, \tag{3}$$

where V is the operating voltage, I_q is the quiescent current, T is the length of time (*e.g.*, 24 hours), $E^{o,s}_{cn}(j)$ is the energy consumption of sensing or communication operation j, and l is the minimum frequency of operation, *e.g.*, once per 30 min.

3) Energy ratio r_p: it is calculated as $r_\mathrm{p} = E_{in}/E_{con}$, which is used to reflect the adequacy of node energy storage.[1] The higher the energy ratio, the more energy the node stores, which is beneficial to the performance of the node.

Constraints. For the optimization objective described in Eqn. (1), we further introduce the following constraints:

[1]When we design a WISE node, we only need to consider the energy ratio r_p in some specific cases in the optimization (*e.g.*, with the minimum level of light source and operating workload, because it is impractical to enumerate all possible situations). The actual energy allocation after deployment is further governed by the duty-cycle regulation method proposed in Section III-C.

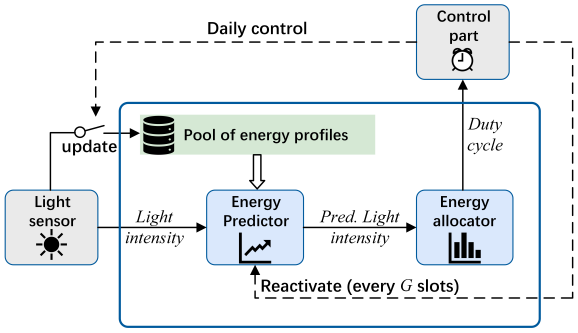

Fig. 7. Duty-cycle regulation method.

Constraint-1 (Energy ratio): we first require that the energy ratio is greater than one, that is, $r_\mathrm{p} > 1$.

Constraint-2 (Cost): the total cost of the selected components should be within the budget b, that is, $\sum_i c_i < b$, where c_i is the price of component i.

Constraint-3 (Capacity of energy storage): the capacity E_{sc} of the supercapacity should be larger than the minimum energy income volume per day, that is, $E_{sc} > E_{in}$.

Summary. The above component selection scheme is a general design that may involve various energy-related components. Developers can use the factor w in Eqn. (1) to balance the node design between node cost and performance, and optimize the objective function of Eqn. (1) to obtain the optimal result of the decision variable $\mathrm{p} = \{p_i\}$ under the above three constraints, where p_i is the parameter selected for component i.

C. Duty-Cycle Regulation

After the hardware design is completed, we introduce the duty-cycle regulation method as shown in Fig. 7 to further manage the harvested energy for sensing and communication.

1) Energy income prediction: Similar to existing energy-harvesting nodes [14], [47], we also regularly predict the energy that will be harvested for the rest of the day [5], based on which we further design a mechanism to update the duty cycle for sensing and communication. To this end, in WISE, we maintain and update a set of energy income profiles (average energy income at different time slots of the day, *e.g.*, one slot is 30 minutes). To determine the duty cycle for sensing and communication, we need to predict the amount of energy to be harvested during the rest of the day. To do this, we will choose the profile that is most similar to the energy harvesting already experienced during the day to estimate the energy income for the rest of the day. Specifically, at time t, the predicted energy income $\hat{E}_{t+i}$ for time slot $t+i$ is calculated as follows:

$$\hat{E}_{t+i} = \begin{cases} \gamma_i \times E_t + (1-\gamma_i) \times E^f_{t+i}, & \text{if } \ i \le G, \\ E^f_{t+i} & \text{if } \ i > G. \end{cases} \tag{4}$$

where $\hat{E}_{t+i}$ is the weighted average of the energy income E_t in the current slot t and the energy income E^f_{t+i} in the future slot $(t+i)$ according to the selected profile E^f (the selected profile is the one in the pool that is most similar to the observed light changes on that day). Factor γ_i is a decay factor $\gamma_i = \alpha \times (1 - \frac{i-1}{G})$, where α is a parameter to be set in the implementation and G is the time interval (number of

TABLE I
SOLAR PANELS AND SUPERCAPACITORS SELECTED AT EACH NODE.

#	Solar panel	Supercapacitor	Cost (USD)	r_{p}
A	KXOB081K06TF (23mm×25mm)	LIC0813Q3R8106 (10 F)	8.89	1.3674
B (Default)	SM141K05TF (22mm×35mm)	LIC0813Q3R8206 (20 F)	9.47	1.8315
C	SM141K07TF (23mm×50mm)	LIC0820Q3R8406 (40 F)	11.84	2.7348

slots) for launching the next prediction and each slot is 0.5 hours in our current design. For the near future (*e.g.*, $i \leq G$), we apply the actual energy income in the current slot to adjust the records in the selected profile as the prediction result in Eqn. (4); otherwise (*e.g.*, $i > G$), we only use the record of the profile as the prediction result for the next energy allocation and make adjustments after making a new prediction.

2) Duty-cycle updates: Based on the predicted energy income, we can estimate the total energy E_t available for the rest of the day as follows:

$$E_t \quad = \quad E_t^{sc} + \sum\nolimits_{j=1}^{N-t} \hat{E}_{t+j}, \tag{5}$$

where E_t^{sc} is the current energy in the supercapacitor and $\sum_{j=1}^{N-t} \hat{E}_{t+j}$ is the energy that is expected to be harvested in the remaining $N - t$ time slots today, where N is the total number of time slots per day. We set the duty cycle by maximizing the sensing and communication frequency within the E_t budget. The duty cycle is updated every G time slots after a new prediction is conducted. Finally, at the beginning of each new day (*i.e.*, 0:00 AM), the RTC initiates a profile pool update, which consolidates the previous day's energy profile to overwrite the previous memory.

IV. IMPLEMENTATION

A. Hardware

The printed circuit board (PCB) size of the WISE node is approximately 36.1mm×36.7mm, as shown in Fig. 1, which is small and easy to deploy. Below, we introduce the details of each component involved in our implementation.

Energy-related components. In Section III-B, we propose an optimization scheme to select various energy-related components. Since solar panels and supercapacitors are the most important components affecting the node performance, we focus on selecting them in the current WISE as a proof-of-concept.[2]

We develop three WISE nodes, denoted as nodes (#A) to (#C), with different energy-related components. The solar panel (SM141K05TF) and supercapacitor (LIC0813Q3R8206) of node (#B) are selected through our optimization to balance performance and cost, as shown in Table I, which is the default node configuration in our evaluation.[3] The cost of these two components is 9.47 USD. Based on the node (#B), we further develop nodes (#A) and (#C) using lower-end and higher-end components (*e.g.*, solar panel and supercapacitor), respectively, to examine their performance differences. Taking a typical 400 Lux indoor office environment as an example (see Section V for details), node (#B) has an energy income/consumption ratio r_{p} of about 1.83. Node (#A) has a lower-end solar panel and supercapacitor, with a lower r_{p} of 1.37, while node (#C) has a higher r_{p} of 2.73 using more expensive components. Table I summarizes the details of each node.

[2]We selected mainstream solar panels and supercapacitors with a unit cost of <10 USD as candidate sets, and then conducted the component selection.

[3]We set $w = 0.98$ in the optimization for node (#B). To provide more energy storage buffer, we use the daily average energy income rather than the minimum one in Constraint-3 to select the supercapacitor in our implementation.

TABLE II
DEFAULT LORA PARAMETERS USED IN THE EVALUATION.

SF	BW	CR	f_c	P_{Tx}	Preamble	Data length
8	125 KHz	4/5	915.125 MHz	10 dBm	20 Symbols	25 Bytes

Other energy-related components required for WISE include charger and regulator. Since they do not directly affect node performance, they can be selected as long as they can provide sufficient operating voltage. Therefore, we do not involve them in the above optimization and adopt the widely used TI BQ25570 power management integrated circuit, which integrates a boost charger and a buck regulator to charge the supercapacitor and provide a stable power supply for the workload in WISE. Considering the operating voltage of the workload (2.82 V) and the maximum voltage tolerance of the supercapacitor (3.8 V), the charging and discharging voltage thresholds of the supercapacitor are set to 2.85 V and 3.8 V.

Control & computing components. The control part is embedded with ultra-low power Micro Crystal RV3028-C7 RTC (real-time clock) for timekeeping during sleep. It has a wide operating voltage range and is suitable for direct power supply by the supercapacitor with unstable voltage (2.85–3.8V).

On the other hand, we use the STM32WLE5CCU6 32-bit ARM Cortex-M4 microcontroller with 64KB SRAM and 256KB Flash in the current WISE. We did not choose the typical MSP430FR5994 microcontroller because its I/O speed is not sufficient to support more advanced sensors such as the image sensor involved in our implementation.

Sensors & communication modules. We reserve a set of interfaces on each node to install different sensors. In the current implementation, we choose two types of sensors to evaluate the system performance. The first one is the BH1750 light sensor (<0.4 mW @3V) with a range from 1 to 65535 Lux and a resolution of 4 Lux. This sensor reads the illumination of the surrounding environment with an operating current of 120–190 μA, which can also be used for our duty-cycle regulation method. To introduce a more challenging configuration, we further install the HM01B0 low-power image sensor (∼6 mW @3V). It generates a quarter VGA (QQVGA) image data frame (160×120 pixels, 8-bit depth) for event detection [28], with an operating current of 2.02 mA.

The STM32WLE5CCU6 microcontroller integrates an on-chip LoRa transceiver peripheral equivalent to the Semtech SX126X, which is used in the current WISE for communication, such as transmitting sensor data and node status back to the gateway (a Raspberry Pi-based Waveshare SX1302 LoRa gateway in the evaluation). We use the parameters in Table II

as the default LoRa settings, including spreading factor (SF), bandwidth (BW), coding rate (CR), center frequency (f_c), transmission power (P_{Tx}), and preamble length, and we will further vary the LoRa parameters to study their impact on the overall system performance in the evaluation.

B. Software

Next, we introduce the settings of key parameters in the duty-cycle regulation method (Section III-C) as follows. (1) The number of energy profiles D. Each profile consumes 96 bytes of FLASH memory. We empirically set $D = 5$ to balance profile diversity and storage overhead. (2) The decay factor α. This factor may affect the prediction of energy income. After multiple simulations, α was set to 0.5 to minimize energy income prediction's mean absolute percentage error (MAPE). (3) The interval G for starting prediction. We set $G = 5$ empirically in the current WISE, which is equivalent to 2.5 ($= 5 \times 0.5$) hours. (4) The ratio between sensing and communication. Since sensing consumes less energy than communication, we allow multiple sensings to be performed between two consecutive transmissions. By default, we set this ratio to 10, that is, 10 sensings are performed before the next transmission.[4]

V. Evaluation

A. Experimental Setup

Deployments. As shown in Fig. 8, we evaluate WISE for 125 hours in two typical IoT scenarios under weak light sources:

- *Indoor office*: we first deploy WISE nodes in an indoor office. The only light source is the fluorescent lamps on the roof. During the experiment, the light is on from 10:00 to 23:00. The default distance between the nodes and the light source is two meters approximately. The average illumination is about 400 Lux when the light is on.
- *Outdoor woods*: we also deploy WISE nodes outdoors in the woods, which can collect sunlight for about 12 hours during the day (*e.g.*, 6:30–18:30). Due to the shadows of the woods, the average illumination is weaker (about 560 Lux) compared to the intensity of normal sunlight.

Baselines. We compare WISE with the following baselines:

- *SMARTON* [28]: a state-of-the-art sensor node design that uses an MCU to control the active/sleep state with RTC timekeeping. Moreover, four power-hungry MOSFETs are used to maintain the power supply. It controls the duty cycle by Q-learning based on light intensity and voltage.
- *ACES* [10]: a state-of-the-art sensor node design that uses an MCU as a timer to control the active/sleep states of the node. It sets the duty cycle by looking up a pre-trained Q-learning table also based on light intensity and voltage.

We implement the two baseline nodes using the same set of components as node (#B), but for evaluation purposes, we follow their hardware architectures [10], [28]. Except for the energy-harvesting components, all other components are identical across our nodes and baselines for fair comparison.

[4]When we calculate the energy consumption E_{cn} in Eqn. (3) to select energy-related components, the energy consumption $E_{cn}^{o,s}(j)$ of each sensing task is the energy consumption of each sensing task multiplied by this ratio.

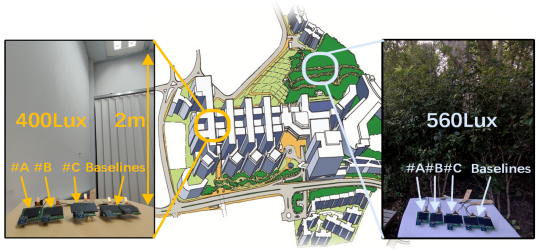

Fig. 8. Indoor and outdoor experimental scenarios.

Metrics. We compare the performance of WISE with two baselines based on the following metrics:

- *Communication rate*: the average number of communications per hour to send data back to the gateway. A higher communication rate indicates more efficient energy use and greater responsiveness.
- *Energy efficiency*: the ratio of task energy consumption (for sensing and communication) per hour to the total consumed energy stored in the supercapacitor. The higher the efficiency, the less energy is wasted.

B. Overall Performance

Performance comparison. We compare the performance 36 hours after nodes are started (also marked later in the detailed traces of Fig. 11 and Fig. 12) to ensure that the learning or prediction of different methods becomes relatively stable. Fig. 9(a) first compares the communication rates of different methods. In indoor scenarios, WISE improves the communication rate by 69.7% and 120.0% compared to SMARTON and ACES, respectively. In outdoor scenarios, the improvement increases to 185.2% and 77.8% compared to SMARTON and ACES, respectively. Fig. 9(b) further shows the comparison of the energy efficiency metric. In the indoors, WISE outperforms SMARTON and ACES by 67.5% and 85.1%, respectively, and in the outdoors, WISE outperforms SMARTON and ACES by 192.0% and 64.3%, respectively.

WISE outperforms both baselines, especially in the outdoors. The reason is that outdoor light intensity varies more dynamically, making energy harvesting unstable and challenging. Our node architecture design and duty-cycle regulation method make WISE work more robustly and efficiently, and we will provide quantitative analysis next.

Performance analysis. To reveal this, we use the LPT2020 power monitor to track the operating current of WISE drawn from the supercapacitor. Fig. 10(a) shows the current variation in different work modes (the operating voltage is 3 V). In the first few seconds, the charger is off and the quiescent current is extremely small, about 60 nA (enlarged in Fig. 10(c)). Subsequently, the node is activated to operate, where the peak current can reach 4 mA (for sensing) and 38 mA (for communication), and the corresponding energy consumption is about 3.3 mJ and 16.2 mJ, respectively. After that, the node gradually reduces the power supply to the workload. To this end, the control part works for about two seconds, with an

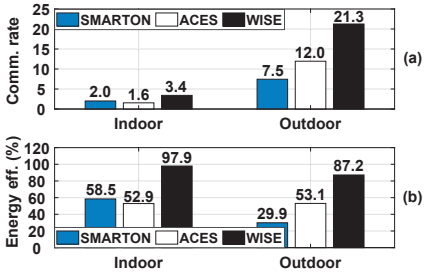

Fig. 9. Overall performance of the three methods in terms of (a) average communication rate (per hour) and (b) energy efficiency.

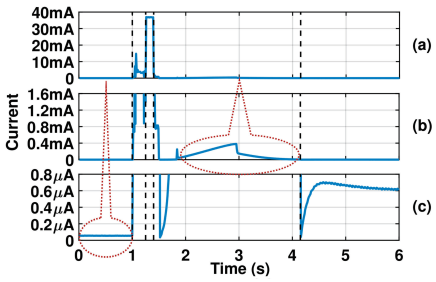

Fig. 10. Working current of WISE (a) overall, (b) zoomed in for 2 to 4 seconds (in the μA level), and (c) zoomed in for the first second (in the nA level).

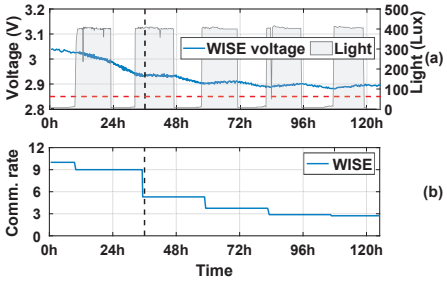

Fig. 11. Indoor experimental process of (a) node voltage and light intensity fluctuations and (b) communication task rate changes on WISE.

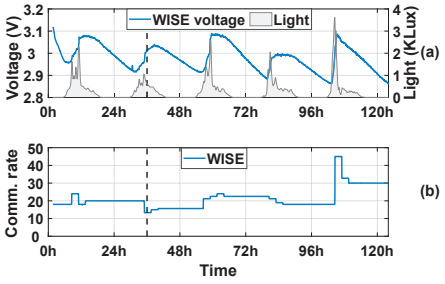

Fig. 12. Outdoor experimental process of (a) node voltage and light intensity fluctuations and (b) communication task rate changes on WISE.

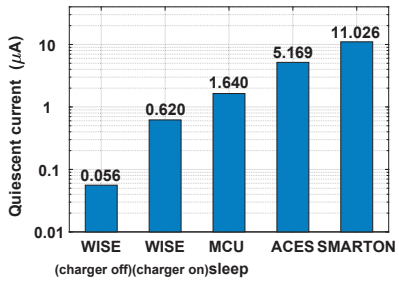

Fig. 13. Comparison of quiescent current for different modes of WISE, sleep mode of the MCU, and two baselines in the log scale.

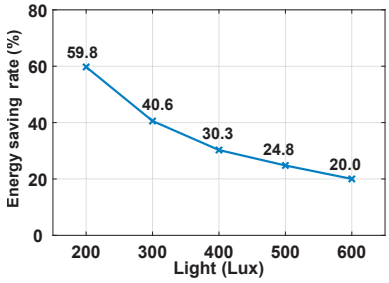

Fig. 14. Rate of the quiescent consumption saved by WISE hardware (compared to ACES) to the harvested energy under different light intensities.

average current of about 150 μA (enlarged in Fig. 10(b)), that is, from 2 to 4 seconds. Finally, the node enters sleep mode (charger on) with a current of about 600 nA. In summary, when the node is not in active mode, the energy consumption of WISE is extremely low, thereby reserving more collected energy for tasks in active mode. As a result, WISE can operate efficiently and stably under weak light sources compared to other baselines, whose quiescent current is larger than 5 μA.

Runtime node statistics. In addition to the quiescent current from our node architecture design, we further show how the duty-cycle regulation method behaves. As mentioned in "Performance Comparison", we skip the first 36 hours in the performance comparison to wait for the method on each node to become relatively stable. Fig. 11(a) shows the variation of node voltage in the indoor scenario. In the first 36 hours (before the vertical dashed line), the voltage gradually decreases as the communication rate increases, as shown in Fig. 11(b). At this stage, the node's energy is relatively high due to the initial power in the supercapacitor. Therefore, the duty-cycle regulation method will schedule smaller duty-cycle periods, reducing the overall energy. After that, the method gradually converges and schedules most tasks under the constraint of retaining energy above the minimum voltage required by the system (the horizontal red dashed line in Fig. 11(a)). Finally, we can see that the voltage of WISE fluctuates around 2.9 V as the light intensity changes, showing that WISE works stably.

As for the outdoor scenario, the light intensity is higher but less predictable than in the indoor scenario, which makes the duty-cycle regulation more challenging. However, Fig. 12 shows that WISE still works well with a good communication rate. The change of voltage follows a similar pattern to the light intensity, which means that the node balances energy income and consumption. In summary, the duty-cycle regulation method ensures that WISE can work stably over time.

C. Micro-benchmark

Quiescent current in different nodes. To evaluate the effectiveness of the WISE node architecture, we configure the WISE node under different settings and Fig. 13 shows the detailed values of the quiescent current. Specifically, the quiescent current of WISE is only 0.056 μA when the charger is off, and 0.62 μA when the charger is on but the node is inactive. In comparison, the quiescent current of MCU (STM32WLE5CCU6, Stop2+RTC mode, @3V) is 1.64 μA, almost three times that of WISE. For the two baseline methods with more components, WISE further reduces the quiescent current by 88.0–99.5%, as shown in Fig. 13.

Impact of different energy incomes. We then explore the impact of different energy harvesting conditions on system performance. We place WISE in an indoor environment with different light intensities and calculate the rate of the quiescent current consumption saved by the WISE hardware (compared to the better baseline ACES) to the total harvested energy, as shown in Fig. 14. As light intensity increases, the energy-saving rate decreases because the quiescent current is constant regardless of light intensity. However, WISE achieves energy savings of 20.0–24.8% at weak light levels (500–600 Lux) and up to 59.8% at very low light (200 Lux). This demonstrates WISE's effectiveness in optimizing energy-harvesting IoT nodes under low-light conditions.

Impact of energy-related components. Fig. 15 shows the communication rate and energy efficiency achieved by different types of WISE nodes using different solar panels and

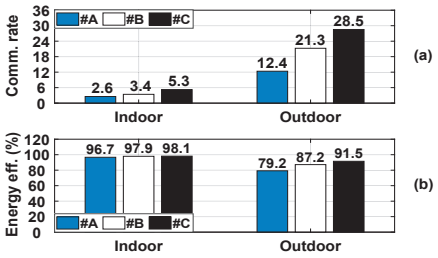

Fig. 15. Performance comparison of WISE using different energy-related components in terms of (a) communication rate and (b) energy efficiency.

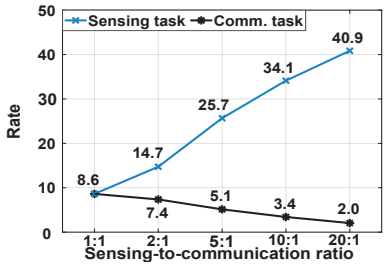

Fig. 16. Average sensing task rate and communication task rate of WISE under different sensing-to-communication ratios (@indoor 400 Lux).

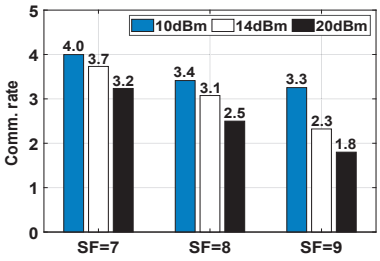

Fig. 17. Average communication rate of WISE under different LoRa spreading factor and transmission power configurations (@indoor 400 Lux).

supercapacitors, as listed in Table I, where nodes (#A) and (#C) prioritize cost and performance, respectively, and node (#B) has a more balanced setting. In Fig. 15(a), the communication rates of nodes (#A), (#B), and (#C) increase from 2.6 to 5.3 per hour in indoor scenarios and from 12.4 to 28.5 per hour in outdoor scenarios, respectively. The communication rate increases proportionally to the node cost, while the energy efficiency has a similar trend, as shown in Fig. 15(b). Therefore, our proposed energy-related component selection scheme can effectively balance node cost and performance.

Impact of sensing-to-communication ratio. This ratio defines the number of times sensing is performed between two consecutive communications, and we set it to 10 by default in WISE. Fig. 16 shows that when the ratio is reduced, more energy can be saved for communication, but the sensing frequency will be reduced; vice versa. In practical applications, different ratios can be set according to the sensing requirements.

Impact of LoRa configurations. The energy consumption of different LoRa configurations, *i.e.*, spreading factor (SF) and transmission power (P_{Tx}), varies [49] and hence can affect the communication rate of WISE. We test the communication rates *w.r.t.* different LoRa configurations, by varying SF from 7 to 9 and P_{Tx} from 10 dBm to 20 dBm in the indoor environment, as shown in Fig. 17. The larger SF and higher P_{Tx} require more energy for each LoRa transmission, leading to a lower communication rate, *e.g.*, the average communication rate decreases from 4 to 3.2 for different P_{Tx} values when SF is 7. The popular setting, *e.g.*, SF is 8 and P_{Tx} is 10 dBm, can also achieve good communication rate performance on WISE.

VI. Related Work

Deploying IoT systems. Sustainability is the primary requirement for IoT system deployment [30]. To this end, various duty-cycle techniques and low-power hardware designs have been proposed to effectively operate IoT nodes alternately between "active" and "sleep" states, thereby improving energy efficiency [6] and extending node lifetime [21], [43], [44]. Recently, the system scalability has also attracted great attention. Compared with traditional Bluetooth and Zigbee, emerging technologies such as LoRa [38] offer promising long-range transmission and low-power consumption under low duty-cycle conditions [12], [18], [25], [41], [46], making them prevalent in IoT deployments [40], [42]. However, these existing solutions are mainly designed for nodes with reliable battery energy supply [7]. When the number of nodes is large, the cost of replacing or recharging batteries is very high, making it difficult for IoT systems to work continuously and autonomously.

Harvesting energy. To overcome this problem, many works have studied how to harvest energy to power IoT nodes. For example, an active research topic is to harvest energy from radio frequency (RF) signals [26], *e.g.*, RFID [23], [37], [52], Wi-Fi [22], and LoRa [16], [35]. However, due to the high cost of RF hardware support and the short distance of RF energy [19], light is a more suitable energy source for IoT nodes [36], [51]. Although some advanced materials for harvesting energy from light have been developed, such as perovskite solar cells [13], they are mainly in the laboratory stage and have not yet been mass-produced. Our design is not limited to solar panels. In the future, when these new energy-harvesting materials become available, we can apply them to WISE.

To fully utilize the harvested energy, intermittent computing research [9], [17], [50] aims to perform computation-oriented tasks efficiently [29] or design key services such as energy storage [8], device discovery [15], sensing managing [50], *etc.* Duty-cycle management of energy-harvesting nodes has also been studied [20], such as prediction-free methods [34], [48], prediction-allocation methods [4], [14], [32] and recent reinforcement learning based methods [1], [10], [11], [28]. However, they rarely study how to optimize the node architecture and duty cycle to cover the important segment of IoT deployment scenarios with weak light sources.

VII. Conclusion

This paper presents WISE to demonstrate the feasibility of using small solar panels to power IoT nodes autonomously in weak light environments. We propose a new IoT node design with an ultra-low power architecture and a novel timing supply control part that drastically reduces the quiescent current. We also design an optimization scheme to select energy-related onboard components and an energy-aware scheduling method to operate the node. Evaluations show significant improvements compared to the state-of-the-art IoT node designs.

Acknowledgment

This work is supported by the National Key R&D Program of China 2023YFB2904000, the NSFC Grant No.62302383 and the GRF grant from Research Grants Council of Hong Kong (CityU 11202623 and CityU 11205624). The corresponding author is Zhenjiang Li.

REFERENCES

[1] F. A. Aoudia, M. Gautier, and O. Berder. Rlman: An energy manager based on reinforcement learning for energy harvesting wireless sensor networks. *IEEE Transactions on Green Communications and Networking*, 2018.

[2] I. J. Ausprey, F. L. Newell, and S. K. Robinson. Adaptations to light predict the foraging niche and disassembly of avian communities in tropical countrysides. *Ecology*, 2021.

[3] Bluetooth technology overview. https://www.bluetooth.com/learn-about-bluetooth/tech-overview/.

[4] B. Buchli, F. Sutton, J. Beutel, and L. Thiele. Dynamic power management for long-term energy neutral operation of solar energy harvesting systems. In *Proc. of ACM SenSys*, 2014.

[5] A. Cammarano, C. Petrioli, and D. Spenza. Pro-energy: A novel energy prediction model for solar and wind energy-harvesting wireless sensor networks. In *Proc. of IEEE MASS*, 2012.

[6] J. Cao, J. Chen, C. Lin, Y. Liu, K. Wang, and Z. Li. Practical gaze tracking on any surface with your phone. *IEEE Transactions on Mobile Computing*, 2024.

[7] Z. Cao, Y. He, and Y. Liu. L2: Lazy forwarding in low duty cycle wireless sensor networks. In *Proc. of IEEE INFOCOM*, 2012.

[8] A. Colin, E. Ruppel, and B. Lucia. A reconfigurable energy storage architecture for energy-harvesting devices. In *Proc. of ACM ASPLOS*, 2018.

[9] J. De Winkel, H. Tang, and P. Pawełczak. Intermittently-powered bluetooth that works. In *Proc. of ACM MobiSys*, 2022.

[10] F. Fraternali, B. Balaji, Y. Agarwal, and R. K. Gupta. Aces: Automatic configuration of energy harvesting sensors with reinforcement learning. *ACM Transactions on Sensor Networks*, 2020.

[11] F. Fraternali, B. Balaji, D. Sengupta, D. Hong, and R. K. Gupta. Ember: energy management of batteryless event detection sensors with deep reinforcement learning. In *Proc. of ACM SenSys*, 2020.

[12] A. Gamage, J. Liando, C. Gu, R. Tan, M. Li, and O. Seller. Lmac: Efficient carrier-sense multiple access for lora. *ACM Transactions on Sensor Networks*, 2023.

[13] D. Gao, B. Li, Z. Li, X. Wu, S. Zhang, D. Zhao, X. Jiang, C. Zhang, Y. Wang, Z. Li, et al. Highly efficient flexible perovskite solar cells through pentylammonium acetate modification with certified efficiency of 23.35%. *Advanced Materials*, 2023.

[14] K. Geissdoerfer, R. Jurdak, B. Kusy, and M. Zimmerling. Getting more out of energy-harvesting systems: Energy management under time-varying utility with preact. In *Proc. of ACM/IEEE IPSN*, 2019.

[15] K. Geissdoerfer and M. Zimmerling. Bootstrapping battery-free wireless networks: Efficient neighbor discovery and synchronization in the face of intermittency. In *Proc. of USENIX NSDI*, 2021.

[16] X. Guo, L. Shangguan, Y. He, J. Zhang, H. Jiang, A. A. Siddiqi, and Y. Liu. Aloba: Rethinking on-off keying modulation for ambient lora backscatter. In *Proc. of ACM SenSys*, 2020.

[17] J. Hester and J. Sorber. Flicker: Rapid prototyping for the batteryless internet-of-things. In *Proc. of ACM SenSys*, 2017.

[18] N. Hou, X. Xia, and Y. Zheng. Don't miss weak packets: Boosting lora reception with antenna diversities. *ACM Transactions on Sensor Networks*, 2023.

[19] K. Huang and X. Zhou. Cutting the last wires for mobile communications by microwave power transfer. *IEEE Communications Magazine*, 2015.

[20] A. Kansal, J. Hsu, S. Zahedi, and M. B. Srivastava. Power management in energy harvesting sensor networks. *ACM Transactions on Embedded Computing Systems*, 2007.

[21] G. Kazdaridis, N. Sidiropoulos, I. Zografopoulos, P. Symeonidis, and T. Korakis. Nano-things: Pushing sleep current consumption to the limits in iot platforms. In *Proc. of ACM IoT*, 2020.

[22] B. Kellogg, A. Parks, S. Gollakota, J. R. Smith, and D. Wetherall. Wi-fi backscatter: Internet connectivity for rf-powered devices. In *Proc. of ACM SIGCOMM*, 2014.

[23] S. Li, Q. Meng, Y. Bai, C. Zhang, Y. Song, S. Li, and L. Lu. Go beyond rfid: Rethinking the design of rfid sensor tags for versatile applications. In *Proc. of ACM MobiCom*, 2023.

[24] Y. Li, N. J. Grabham, S. P. Beeby, and M. Tudor. The effect of the type of illumination on the energy harvesting performance of solar cells. *Solar Energy*, 2015.

[25] J. C. Liando, A. Gamage, A. W. Tengourtius, and M. Li. Known and unknown facts of lora: Experiences from a large-scale measurement study. *ACM Transactions on Sensor Networks*, 2019.

[26] V. Liu, A. Parks, V. Talla, S. Gollakota, D. Wetherall, and J. R. Smith. Ambient backscatter: Wireless communication out of thin air. *ACM SIGCOMM computer communication review*, 2013.

[27] B. Lucia, B. Denby, Z. Manchester, H. Desai, E. Ruppel, and A. Colin. Computational nanosatellite constellations: Opportunities and challenges. *ACM GetMobile: Mobile Computing and Communications*, 2021.

[28] Y. Luo and S. Nirjon. Smarton: Just-in-time active event detection on energy harvesting systems. In *Proc. of IEEE DCOSS*, 2021.

[29] H. R. Mendis, C.-K. Kang, and P.-c. Hsiu. Intermittent-aware neural architecture search. *ACM Transactions on Embedded Computing Systems*, 2021.

[30] L. Mo, Y. He, Y. Liu, J. Zhao, S.-J. Tang, X.-Y. Li, and G. Dai. Canopy closure estimates with greenorbs: Sustainable sensing in the forest. In *Proc. of ACM SenSys*, 2009.

[31] S. Mosavat, M. Zella, M. Handte, A. J. Golkowski, and P. J. Marrón. Experience: Aristotle: wake-up receiver-based, star topology batteryless sensor network. In *Proc. of ACM/IEEE IPSN*, 2023.

[32] D. K. Noh and K. Kang. Balanced energy allocation scheme for a solar-powered sensor system and its effects on network-wide performance. *Journal of Computer and System Sciences*, 2011.

[33] V. Pecunia, L. G. Occhipinti, and R. L. Hoye. Emerging indoor photovoltaic technologies for sustainable internet of things. *Advanced Energy Materials*, 2021.

[34] S. Peng and C. P. Low. Prediction free energy neutral power management for energy harvesting wireless sensor nodes. *Ad Hoc Networks*, 2014.

[35] Y. Peng, L. Shangguan, Y. Hu, Y. Qian, X. Lin, X. Chen, D. Fang, and K. Jamieson. Plora: A passive long-range data network from ambient lora transmissions. In *Proc. of ACM SIGCOMM*, 2018.

[36] G. Peruzzi and A. Pozzebon. A review of energy harvesting techniques for low power wide area networks (lpwans). *Energies*, 2020.

[37] A. P. Sample, D. J. Yeager, P. S. Powledge, A. V. Mamishev, and J. R. Smith. Design of an rfid-based battery-free programmable sensing platform. *IEEE Transactions on Instrumentation and Measurement*, 2008.

[38] Semtech lora technology overview. https://www.semtech.com/lora.

[39] P. Sparks. The route to a trillion devices. *White Paper, ARM*, 2017.

[40] Z. Sun, T. Ni, H. Yang, K. Liu, Y. Zhang, T. Gu, and W. Xu. Flora: Energy-efficient, reliable, and beamforming-assisted over-the-air firmware update in lora networks. In *Proc. of ACM/IEEE IPSN*, 2023.

[41] Z. Sun, H. Yang, K. Liu, Z. Yin, Z. Li, and W. Xu. Recent advances in lora: A comprehensive survey. *ACM Transactions on Sensor Networks*, 2022.

[42] S. Tong, J. Wang, J. Yang, Y. Liu, and J. Zhang. Citywide lora network deployment and operation: Measurements, analysis, and implications. In *Proc. of ACM SenSys*, 2023.

[43] J. Wang, Z. Cao, X. Mao, X.-Y. Li, and Y. Liu. Towards energy efficient duty-cycled networks: Analysis, implications and improvement. *IEEE Transactions on Computers*, 2015.

[44] J. Wang, Z. Cao, X. Mao, and Y. Liu. Sleep in the dins: Insomnia therapy for duty-cycled sensor networks. In *Proc. of IEEE INFOCOM*, 2014.

[45] K. Wang, J. Cao, Z. Zhou, and Z. Li. Swapnet: Efficient swapping for dnn inference on edge ai devices beyond the memory budget. *IEEE Transactions on Mobile Computing*, 2024.

[46] X. Xia, Q. Chen, N. Hou, Y. Zheng, and M. Li. Xcopy: Boosting weak links for reliable lora communication. In *Proc. of ACM MobiCom*, 2023.

[47] N. Yamin and G. Bhat. Uncertainty-aware energy harvest prediction and management for iot devices. *ACM Transactions on Design Automation of Electronic Systems*, 2023.

[48] F. Yang, A. S. Thangarajan, W. Joosen, C. Huygens, D. Hughes, G. S. Ramachandran, and B. Krishnamachari. Astar: Sustainable battery free energy harvesting for heterogeneous platforms and dynamic environments. In *Proc. of EWSN*, 2019.

[49] K. Yang, M. Liu, and W. Du. Ralora: Rateless-enabled link adaptation for lora networking. *IEEE/ACM Transactions on Networking*, 2024.

[50] K. S. Yıldırım, A. Y. Majid, D. Patoukas, K. Schaper, P. Pawelczak, and J. Hester. Ink: Reactive kernel for tiny batteryless sensors. In *Proc. of ACM Sensys*, 2018.

[51] S. Zeadally, F. K. Shaikh, A. Talpur, and Q. Z. Sheng. Design architectures for energy harvesting in the internet of things. *Renewable and Sustainable Energy Reviews*, 2020.

[52] C. Zhao, Z. Li, H. Ding, G. Wang, W. Xi, and J. Zhao. Rf-wise: Pushing the limit of rfid-based sensing. In *Proc. of IEEE INFOCOM*, 2022.